

Separated Fringe Packet Observations with the CHARA Array II: ω Andromeda, HD 178911, and ξ Cephei.

C.D. Farrington, T.A. ten Brummelaar

The CHARA Array, Mt. Wilson Observatory, Mt. Wilson, CA 91023

farrington@chara-array.org, theo@chara-array.org

B.D Mason, W.I Hartkopf

US Naval Observatory, 3450 Massachusetts Avenue NW, Washington, DC 20392-5420

bdm@usno.navy.mil, wih@usno.navy.mil

D. Mourard

Université de Nice Sophia Antipolis, CNRS, Laboratoire J.L. Lagrange, Observatoire de la
Côte d'Azur - BP4209, 06304 Nice cedex, France

denis.mourard@oca.eu

E. Moravveji

Instituut voor Sterrenkunde, KU Leuven, Celestijnenlaan 200D, 3001, Leuven, Belgium

Ehsan.Moravveji@ster.kuleuven.be

H.A. McAlister

Center for High Angular Resolution Astronomy, Georgia State University, P.O. Box 3969,
Atlanta, GA 30302-3969

hal@chara.gsu.edu

N.H. Turner, L. Sturmann, J. Sturmann

The CHARA Array, Mt. Wilson Observatory, Mt. Wilson, CA 91023

nils@chara-array.org, sturmann@chara-array.org, judit@chara-array.org

Received _____; accepted _____

ABSTRACT

When observed with optical long-baseline interferometers (OLBI), components of a binary star which are sufficiently separated produce their own interferometric fringe packets; these are referred to as Separated Fringe Packet (SFP) binaries. These SFP binaries can overlap in angular separation with the regime of systems resolvable by speckle interferometry at single, large-aperture telescopes and can provide additional measurements for preliminary orbits lacking good phase coverage, help constrain elements of already established orbits, and locate new binaries in the undersampled regime between the bounds of spectroscopic surveys and speckle interferometry. In this process, a visibility calibration star is not needed, and the separated fringe packets can provide an accurate vector separation. In this paper, we apply the SFP approach to ω Andromeda, HD 178911, and ξ Cephei with the CLIMB three-beam combiner at the CHARA Array. For these systems we determine component masses and parallax of $0.963 \pm 0.049 M_{\odot}$ and $0.860 \pm 0.051 M_{\odot}$ and 39.54 ± 1.85 milliarcseconds (mas) for ω Andromeda, for HD 178911 of $0.802 \pm 0.055 M_{\odot}$ and $0.622 \pm 0.053 M_{\odot}$ with 28.26 ± 1.70 mas, and masses of $1.045 \pm 0.031 M_{\odot}$ and $0.408 \pm 0.066 M_{\odot}$ and 38.10 ± 2.81 mas for ξ Cephei.

Subject headings: techniques: high angular resolution — techniques: interferometric — stars: individual (ω Andromeda, HD 178911, ξ Cephei) — binaries: close — infrared: stars

1. Introduction

Long-baseline interferometric telescope arrays are well-suited for observing binaries with angular separations in the sub-millarcsecond regime using the traditional interferometric visibility method [for examples, see Armstrong (1992), Boden et al (1999), Hummel et al. (1995), and Raghavan et al. (2009)]. Another approach [Dyck et al. (1995), Lane & Muterspaugh (2004), Bagnuolo et al. (2006), ten Brummelaar et al. (2011)] applies to stellar systems where the components of a binary are sufficiently far apart in projected angular separation that their fringe packets do not overlap and the visibility fitting approach is not relevant. This paper follows Farrington et al. (2010) (hereafter referred to as Paper I) presenting the results from a program of separated fringe packet (SFP) observations of spectroscopic and visual binary star systems made with the CHARA Array at Mount Wilson Observatory (ten Brummelaar et al. 2005). Paper I contained the systems χ Draconis, HD 184467, and HD 198084, and presented new observations, orbits, and masses for each system, and a variant of this technique is presented for triple systems in O’Brien et al. (2011). As part of this ongoing effort, we present here 150 new vector measurements of ω Andromeda, HD 178911, and ξ Cephei that are combined into 60 positional observations of the components of these systems. With this second paper, we have refined the process of data collection and reduction to incorporate the increased capacity and efficiency of the CLIMB (CLassic Interferometry with Multiple Baselines) beam combiner (ten Brummelaar et al. 2013).

2. Observational Overview

Data were routinely taken on the CHARA Array’s three largest baselines (S1-E1-W1) and other intermediate baselines when the preferred telescopes were assigned to other simultaneous observing experiments. A list of observations for ω Andromeda, HD 178911,

and ξ Cephei taken with the CHARA Array, along with baselines used, is given in Table 1. This table contains the acquired 1-D measurements in columns 3 – 6 and the 2-D positional calculation obtained from the observations in columns 7 – 9. Each 1-D measurement consist of averaged time, length of baseline, and position angle of the projected baseline at the midpoint of the five minute recording sequence and a separation between the peaks of the two average fringe envelopes that have been summed over the course of the data file [see Farrington et al. (2010)]. The 2-D columns represent the combination of all the 1-D data for a given set of observations through the program described in the Data Reduction section below. The exceptions to the above descriptions are those data labeled "VEGA" in the table. These measurements do not use the SFP method but visibility modulation typical for interferometers, and thus do not consist of 1-D vector measurements. Full details of the VEGA instrument can be found in Mourard et al. (2009).

Before 2009, observations for the SFP program were taken as described in Paper I with the CHARA Classic two-beam combiner as described by (ten Brummelaar et al. 2005). All observations after 2009 were taken with the CHARA CLIMB IR pupil-plane three-beam combiner (ten Brummelaar et al. 2013) also through the K' filter. The timespan between observing sessions ranged from as little as a week to more than a year. Orbits for these systems were determined with combined spectroscopic/interferometric solutions as described in Tokovinin et al. (1992); Tokovinin (1993) with all available CHARA, published speckle interferometry data (Hartkopf et al. 2001b), and spectroscopic orbits as described below.

2.1. Characterizing Separated Fringe Packets

The theory, history, errors, and method of utilizing SFP interferometry are discussed in detail in Paper I. Several important changes have been implemented since the publication

of that paper that have increased the accuracy, quality, and speed of the data acquisition with the CHARA Array. In 2009, the new CLIMB three-beam combiner (Sturmann et al. 2010) was built alongside of the previously used CLASSIC two-beam combiner. While primarily built for multiple simultaneous baseline observations to determine closure phase (ten Brummelaar et al. 2013), the SFP project found an alternative use for the combiner, as the primary mode for CLIMB used two dither mirrors working simultaneously at different frequencies and movement parameters narrowed the delay-space being sampled at any given time. If used in its primary mode, this would decrease the 1-D sky coverage of two of the baselines by 25% for the second pair of baselines that include a dither mirror, and 50% for the final pair which is considered the “cross fringe.” In order to retain the largest possible sky coverage, a two-beam mode was added that used the same frequencies and largest possible delay-space search for all three baselines, but only recorded one baseline at a time. With this mode on CLIMB, the amount of time needed to observe one object on all three baselines took less than a quarter of the time required by the method described in Paper I.

2.2. Data Reduction

Most of the data reduction was done with the same method and software as described in Farrington et al. (2010) with the exception of the final stage, the determination of the 2-D location of the companion.

2.2.1. Calculation Method for Astrometry from SFP Data

Each observation of a binary star produces a linear separation of the system on the sky, whose direction is determined by the projection angle of the baseline on the sky and whose distance is determined by the separation of the two fringe packets divided by the

projected baseline length (Farrington et al. 2010). Thus, if we place the primary, as defined by the star that produces the largest fringe packet¹, at the origin, each observation will produce a line, which for observation i we write as

$$y = m_i x + c_i. \quad (1)$$

For any single observation, the position of the secondary (x_s, y_s) can lie anywhere on this line, but for more than one observation the position of the secondary is more restricted. Ideally all of the lines will intersect at the position of the secondary, but of course the presence of noise makes this extremely unlikely. We therefore use the equivalent of a χ^2 minimization.

We write the distance of the secondary from the line defined by observation i as

$$\Delta_i = \sqrt{(x_s - x_p)^2 + (y_s - y_p)^2}, \quad (2)$$

where (x_p, y_p) is the point on the line defining the perpendicular distance between (x_s, y_s) and the line given by

$$x_p = \frac{x_s + m_i y_s - m_i c_i}{1 + m_i^2} \quad (3)$$

and

$$y_p = m_i x_p + c_i. \quad (4)$$

We then say that the χ^2 of any secondary position is given by

$$\chi^2 = \sum_{i=1}^{N_{\text{obs}}} \frac{\Delta_i^2}{\sigma_i^2} \quad (5)$$

¹Note that the star that produces the largest fringe packet is not necessarily the brightest star as the brightest star may be more resolved at the current baseline than the fainter star and its fringe packet is suppressed.

where σ_i^2 is the variance of the linear separation of observation i . Following standard χ^2 analysis, we say that the best estimate for the position of the secondary is given by the values of (x_s, y_s) that minimize χ^2 . Since this is not a true χ^2 measurement the error can not be estimated in the normal way. Instead we use the standard deviation of the perpendicular distances, Δ_i . A program was written in C by T.A. ten Brummelaar that does the above calculations called “SFPAstrom” and a sample output of the resulting fits is displayed in Figure 1.

2.3. Effects of Misalignment

In Paper I, the most prevalent possible sources of error were discussed and all but the piston error were of such a small magnitude that they could essentially be dismissed. It is worth quantifying the potential error in separation of two fringe packets brought about by the misalignment of the optical path from the beam combiner out to the telescope on one arm of the interferometer.

Starting with the configuration in Figure 2, we can calculate the error in path for a single star for a typical misalignment that could occur due to coudé variation in azimuth of approximately 5mm or about 10 arcseconds over the longest baseline. We want to determine χ_1 and χ_2 in terms of the nominal distances (d_1 and d_2), the angle of the telescope, θ , and the misalignment angle, α . From simple geometric identities, it can be shown that:

$$\chi_1 = \frac{d_1 \sin(\frac{\alpha}{2} - \frac{\theta}{2})}{\sin(\frac{3\alpha}{2} - \frac{\theta}{2})} \quad (6)$$

and

$$\chi_2 = \frac{d_2 \sin(\frac{3\alpha}{2} + \frac{\theta}{2})}{\sin(\frac{\alpha}{2} + \frac{\theta}{2})} \quad (7)$$

For the pertinent case where we are observing a binary system that would produce two fringes as described in Paper I, we show that the path difference for the individual

components for a relatively wide realistic case:

$$\chi_1(\theta) + \chi_2(\theta) - \chi_1(\theta + \Delta) - \chi_2(\theta + \Delta) \ll \vec{\rho}_{\mu\text{m}} \quad (8)$$

where Δ is the on-sky separation of the two fringes in milliarcseconds and rearranging Equation 5 from Paper I gives:

$$\vec{\rho}_{\mu\text{m}} = \frac{\vec{\rho}_{\text{mas}} B(m)}{206.265} \quad (9)$$

The solutions for Equation 8 are given in Figure 3 with increasing θ and from 0-10 arcsecond misalignment for a baseline of 300 m and projected binary star separation of 60 mas, show a maximum differential delay that is 3 orders of magnitude smaller than the separation between the two fringes (for this example, the separation of the fringes in microns is approximately $87\mu\text{m}$, and the error due to the largest misalignment approaches $0.08\mu\text{m}$), and thus far smaller than atmospheric piston, the most dominant source of positional error.

3. Results

3.1. ω Andromeda

ω Andromeda = HR 417, HD 8799, spectral types are suggested to be F3V+F5V (Abt 1985; Cowley 1976). The listed B component is faint (12th magnitude at $2''$) and may be optical Burnham (1873, 1887). The system also contains a second pair $2'$ distant, separated by $5''$ with a combined magnitude of 10, designated as components CD, which are optical. No previous astrometric or interferometric observations of the system have been published. All astrometric data taken for this system was obtained on the CHARA Array using CLIMB and the VEGA visible beam combiner (Mourard et al. 2009). VEGA data are not processed through the SFP principle but they used the classical principle of visibility modulation as a function of time, baseline, as in Pan et al. (1990). The spectroscopic orbit used in the combined solution presented here is from Griffin (2011). A simultaneous solution utilizing

all the radial velocity and visual data was carried out with an interactive program developed by Tokovinin et al. (1992); Tokovinin (1993) that computes all 10 orbital elements. This technique employs the method of least squares to yield elements satisfying both radial velocity and astrometric measurements as described in McAlister et al. (1995). The orbital elements from the combined solution are listed in Table 2, along with the orbital χ^2_ν , masses, and orbital parallax calculated from the solution, and Figure 4 shows the relative orbit. The orbital parallax of 39.54 ± 1.85 milliarcseconds (mas) is different from that of Hipparcos (34.94 ± 0.31 mas; van Leeuwen (2008)), probably due to the pair being unresolved and the parallax being biased with the binary separation. The calculated masses are $0.963 \pm 0.049 M_\odot$ and $0.860 \pm 0.051 M_\odot$ for the components and an orbital grade of 1 determined by criteria of the Sixth Orbital Catalog (Hartkopf et al. 2001a).

3.2. HD 178911

HD 178911 = HR 7272, CHR 84Aa,Ab, spectral types are G1V+K1V. Measured diameter is 0.114 mas (Ribas et al. 2003). The AB pair ($16''$, $\Delta m=1.1$) is known as STF2747 and shares a common proper motion. The B component of the wide pair is an extrasolar planet host star (Wittenmyer et al. 2009). The much wider AC pair is known as WAL 105 ($96''$, $\Delta m=4.6$) and is optical. The close Aa,Ab pair was discovered by the CHARA speckle interferometry program in 1985 (McAlister et al. 1987). Summary information for components can be found in the Washington Double Star (WDS) Catalog (Mason et al. 2001). The entry from the Sixth Visual Orbit Catalog [ORB6; Hartkopf et al. (2001a)] is from Hartkopf et al. (2000), and the spectroscopic orbit and first combined solution are from Tokovinin et al. (2000). While the previous orbit included only six visual measurements, our solution is quite similar with reduced errors while including 17 measurements from the CHARA Array, and 10 other subsequent speckle interferometric data points. This

five-fold increase in the number of measures of relative astrometry has a significant impact on the mass and other determinations due to much lower errors. The orbit, presented in Table 3, was computed using the same combined solution technique of (Tokovinin et al. 1992; Tokovinin 1993) listed above deriving all ten orbital parameters as well as orbital χ^2 , component masses, and orbital parallax. Figure 5 plots the previous and current orbital solutions with all measurements previous to this effort. The orbital parallax of 28.26 ± 1.70 milliarcseconds (mas) is different from that of Hipparcos (19.11 ± 2.35 mas; (van Leeuwen 2008)), probably due to the pair being unresolved and the parallax being affected by the binary separation. Using the objective orbit grading scheme described in ORB6 a grade of 1, definitive, has been determined for this pair. As with all other orbits in ORB6, this is based only on the orbital elements and the resolved measures and, therefore, does not take into account the spectroscopic solution which significantly improves the quality. The calculated masses of $0.802 \pm 0.055 M_{\odot}$ and $0.622 \pm 0.053 M_{\odot}$ for the Aa and Ab components, while lower, are within the error margin of the previous solution.

3.3. ξ Cephei A

ξ Cephei A = HR 8417, HD 209790, MCA 69Aa,Ab. The AB (5-8", $\Delta m=2.0$) and AC (110", $\Delta m=8.2$) pairs are both known as STF2863. B shares a common proper motion with A. The C component has only been measured a few times since its discovery in 1925 (Öpik 1932) and its status, whether optical or physical, is unknown. Eggen (1991, 1992) has determined the system to be a member of the IC 2391 supercluster. Summary information for the system can be found in the Washington Double Star (WDS) Catalog (Mason et al. 2001). Hyneck (1938) included the close pair in a list of composite spectrum binaries, and Abt (1961) suggested that it is long-period spectroscopic binary. Vickers & Scarfe (1976) confirmed Abt's suspicion, finding the system to be double-lined with an orbital period of

811 days. From an analysis of colors, Vickers & Scarfe assigned spectral types of A7 for Aa and F5 for Ab, suspecting on the basis of strong lines of strontium and ionized iron that the secondary is a subgiant. The fit to the colors leads to a $\Delta V = 0.3$ magnitudes, a value significantly smaller than that expected for a pair of A7 and F5 dwarfs, lending further support to the evolved nature of the secondary. Vickers & Scarfe also measured the radial velocity of the B component and found it indistinguishable from the γ -velocity of the Aa,Ab system, confirming the common proper motion physicality. The system Aa,Ab was subsequently resolved by speckle interferometry (McAlister 1977) and in McAlister (1980) the first relative orbit was derived from ten speckle observations and compared with the spectroscopic orbit of (Vickers & Scarfe 1976).

The passage of time has quadrupled the number of interferometric measurements, most recently in the separated fringe packet campaign with the CHARA Array, and more importantly, this has increased the phase coverage from 1.3 to 16.4 orbital revolutions. All published observations of the pair are listed in the Fourth Interferometric Catalog (Hartkopf et al. 2001b) including the recent measures by speckle interferometry by Horch et al. (2008, 2010). The orbit, as presented in Table 4 was computed using the same combined solution technique of (Tokovinin et al. 1992; Tokovinin 1993) listed above and plotted in Figure 6. As above, the orbital parallax of 38.10 ± 2.81 mas is different from that of Hipparcos (33.79 ± 1.06 mas; (van Leeuwen 2008)), probably due to the pair being unresolved and the parallax again being biased by the binary separation. Using the objective orbit grading scheme described in ORB6 a grade of 2, good, has been determined for this pair. As above this is based only on the orbital elements and the resolved measures and does not take into account the spectroscopic solution which significantly improves the quality. The masses of $1.045 \pm 0.031 M_{\odot}$ and $0.408 \pm 0.066 M_{\odot}$ for the components are of the same order as the previous solutions but are significantly different from what should be expected from a system with spectral types listed above.

4. Conclusion

As it was suggested in the first paper of this series, the inclusion of the CLIMB beam combiner did significantly increase the accuracy and alacrity of data acquisition for the SFP binary program. The three systems observed in this paper are just the first of many that are available to this technique and the ongoing effort continues to add new spectroscopic binaries that are within the available observation range for orbit determination. It should be noted that for the three systems discussed herein, and χ Draconis from Paper I of this series, the combined orbital solutions provide masses that do not mesh well with the predicted masses assigned from spectral typing. We present these orbits as they are computed, without prejudice to previously quoted spectral types, as the spectral typing and luminosity class determination are beyond the scope of the current investigation. Additionally, five of the six objects from both this discussion and Paper I show significant differences between the orbital parallax calculated here and the Hipparcos parallax measurements due to the binarity unresolved at that time.

The CHARA Array, operated by Georgia State University, was built with funding provided by the National Science Foundation, Georgia State University, the W. M. Keck Foundation, and the David and Lucile Packard Foundation. This research is supported by the National Science Foundation under grant AST 0908253 and AST 1211129 as well as by funding from the office of the Dean of the College of Arts and Science at Georgia State University. This research has made use of the SIMBAD database, operated at CDS, Strasbourg, France. Thanks are also extended to the U. S. Naval Observatory for their continued support of the Double Star Program. We very much appreciate the hard work of Isabelle Tallon-Bosc for the support for this project. This research has made use of the Jean-Marie Mariotti Center LITpro service co-developped by CRAL, LAOG and FIZEAU

(Tallon-Bosc et al. 2008).²

²LITpro software available at <http://www.jmmc.fr/litpro>

REFERENCES

Abt, H., 1961, *ApJS* 6, 37

Abt, H., 1985 *ApJS* 59, 95

Armstrong, J. T., Mozurkewich, D., Vivekanand, M., Simon, R. S., Denison, C. S.,
Johnston, K. J., Pan, X. P., Shao, M., & Colavita, M. M., 1992, *AJ* 104, 241

Bagnuolo, W. G. Jr., Taylor, S. F., McAlister, H. A., ten Brummelaar, T. A., Gies, D. R.,
Ridgway, S. T., Sturmann, J., Sturmann, L., Turner, N. H., & Berger, D. H. 2006,
AJ 131, 2695

Boden, A. F., Lane, B. F., Creech-Eakman, M. J., Colavita, M. M., Dumont, P. J., Gubler,
J., Koresko, C. D., Kuchner, M. J., Kulkarni, S. R., Mobley, D. W., Pan, X. P., Shao,
M., van Belle, G. T., Wallace, J. K., & Oppenheimer, B. R., 1999, *AJ* 527, 360

ten Brummelaar, T. A., McAlister, H. A., Ridgway, S. T., Bagnuolo, W. G. Jr., Turner,
N. H., Sturmann, L., Sturmann, J., Berger, D. H., Ogden, C. E., Cadman, R.,
Hartkopf, W. I., Hopper, C. H., & Shure, M. A. 2005, *ApJ* 628, 453

ten Brummelaar, T. A., O'Brien, D. P., Mason, B. D., Farrington, C. D., Fullerton, A. W.,
Gies, D. R., Grundstrom, E. D., Harkopf, W. I., Matson, R. A., McAlister, H. A.,
McSwain, M. V., Roberts, L. C., Schaefer, G. H., Simn-Daz, S., Sturmann, J.,
Sturmann, L., Turner, N. H., & Williams, S. J., 2011, *AJ* 142, 21

ten Brummelaar, T. A., Sturmann, J., McAlister, H. A., Sturmann, L., Turner, N. H.,
Farrington, C. D., Schaefer, G., Goldfinger, P. J., & Kloppenborg, B., 2012,
Proc. SPIE 8445, 123

ten Brummelaar, T. A., Sturmann, J., Ridgway, S. T., Sturmann, L., Turner, N. H.,

- McAlister, H. A., Farrington, C. D., Beckmann, U., Weigelt, G., & Shure, M.,
Journal of Astronomical Instrumentation, in Press 2013.
- Burnham, S. W., 1873, MNRAS 33, 437
- Burnham, S. W., 1887, Pub. Lick Obs. 1, 45
- Cowley, A. P., 1976, PASP 88, 95
- Dyck, H. M., Benson, J. A., & Schloerb, F. P., 1995, ApJ 110, 1433
- Eggen, O. J., 1991, AJ 102, 2028
- Eggen, O. J., 1992, AJ 104, 2141
- Farrington, C. D., ten Brummelaar, T. A., Mason, B. D., Hartkopf, W. I., McAlister, H. A.,
Raghavan, D., Turner, N. H., Sturmann, L., Sturmann, J., & Ridgway, S. T., 2010,
AJ 139, 2308
- Griffin, R. F., 2011, The Observatory 131, 4, 225
- Hartkopf, W. I., McAlister, H. A., & Franz, O. G. 1989, ApJ 98, 1014
- Hartkopf, W. I., Mason, B. D., McAlister, H. A., Roberts, L. C., Jr., Turner, N. H., ten
Brummelaar, T. A., Prieto, C. M., Ling, J. F., & Franz, O. G., 2000, AJ 119, 3084
- Hartkopf, W. I., Mason, B. D., & Worley, C. E., 2001a, AJ 122, 3472
<http://ad.usno.navy.mil/wds/orb6.html>
- Hartkopf, W. I., McAlister, H. A. & Mason, B. D. 2001b, AJ 122, 3480
<http://ad.usno.navy.mil/wds/int4.html>
- Horch, E. P., van Altena, W. F., Cyr, W. M., Jr., Kinsman-Smith, L., Srivastava, A. &
Zhou, J., 2008, AJ 136, 312

Horch, E. P., Falta, D., Anderson, L. M., DeSousa, M. D., Minitier, C. M., Ahmed, T. & van Altena, W. F., 2010, AJ 139, 205

Hummel, C. A., Armstrong, J. T., Buscher, D. F., Mozurkewich, D., Quirrenbach, A., & Vivekanand, M., 1995, AJ 110, 376

Hummel, C. A., Mozurkewich, D., Armstrong, J. T., Hajian, Arsen R., Elias, N. M., II, & Hutter, D. J., 1998, AJ 116, 2536

Hynek, J. A., 1938, Cont Perkins Obs 1, 10

Lane, B. F. & Muterspaugh, M. W, 2004, ApJ 601, 1129

van Leeuwen, F., 2007, A&A 474, 653

Mason, B. D., Wycoff, G. L., Hartkopf, W. I., Douglass, G. G., & Worley, C. E., 2001, AJ 122, 3466

McAlister, H. A., 1977, ApJ 215, 159

McAlister, H. A., 1980, ApJ 236, 522

McAlister, H. A., Hartkopf, W. I., Hutter, D. J., Shara, M. M., & Franz, O. G., 1987, AJ 93, 183

McAlister, H. A., Hartkopf, W. I., Mason, B. D., Fekel, F. C., Ianna, P. A., Tokovinin, A. A., Griffin, R. F. & Culver, R. B., 1995, AJ 110, 366

Mourard, D., Clause, J. M, Marcotto, A., Perraut, K., Tallon-Bosc, I., Brio, P., Blazit, A., Bonneau, D., Bosio, S., Bresson, Y., Chesneau, O., Delaa, O., Hnault, F., Hughes, Y., Lagarde, S., Merlin, G., Roussel, A., Spang, A., Stee, P., Tallon, M., Antonelli, P., Foy, R., Kervella, P., Petrov, R., Thiebaut, E., Vakili, F., McAlister, H. A., ten

- Brummelaar, T. A., Sturmann, J., Sturmann, L., Turner, N., Farrington, C. D., & Goldfinger, P. J., 2009, *A&A* 508, 1073
- Öpik, E., 1932, *Pub. Tartu Obs.* 27, 5
- O'Brien, D. P., McAlister, H. A., Raghavan, D., Boyajian, T. S., ten Brummelaar, T. A.; Sturmann, J., Sturmann, L., Turner, N. H., & Ridgway, S., 2011 *ApJ* 728, 8
- Pan, X. P., Shao, M., Colavita, M. M., Mozurkewich, D., Simon, R. S., & Johnston, K. J., 1990, *ApJ* 356, 641
- Pourbaix, D. 2000, *ApJS* 145, 215
- Raghavan, D, McAlister, H. A., Torres, G., Latham, D. W., Mason, B. D., Boyajian, T. S., Baines, E. K., Williams, S. J., ten Brummelaar, T.A., Farrington, C. D., Ridgway, S. T., Sturmann, L., Sturmann, J., & Turner, N. H. 2009, *ApJ* 690, 394
- Ribas, I., Solano, E., Masana, E., & Giménez, A., 2003, *A&A* 411, L501
- Sturmann, J., ten Brummelaar, T. A., Sturmann, L., & McAlister, H. A., 2010, *Proc. SPIE* 7734, 119
- Tallon-Bosc, I., Tallon, M., Thiébaud, E., Béchet, C., Mella, G., Lafrasse, S., Chesneau, O., Domiciano de Souza, A., Duvert, G., Mourard, D., Petrov, R., & Vannier, M., 2008, *Proc. SPIE* 7013, 44
- Tokovinin, A. A. 1992, in *Complementary Approaches to Double and Multiple Star Research*, ASP Conf Ser. **32**, IAU Colloquium 135, edited by H.A. McAlister and W.I. Hartkopf, 573
- Tokovinin, A. A. 1993, *Astronomy Letters* 19, 73

Tokovinin, A. A., Griffin, R. F., Balega, Y. Y., Pluzhnik, E. A., & Udry, S., 2000,
Astronomy Letters 26, 116

Vickers, C. R., & Scarfe, C. D., 1976, PASP 88, 944

Wittenmyer, R. A.; Endl, M; Cochran, W. D.; Levison, H. F.; & Henry, G. W., 2009,
ApJS 182, 97

Table 1. CHARA SFP Observations

System	Set	MJD	B(m)	$\vec{\theta}(\circ)$	$\vec{\rho}(\text{mas})$	BY	θ	$\rho(\text{mas})$
ω And	1	54786.29163	329.24	9.76	9.58			
		54786.29637	329.34	8.66	12.03			
		54786.38633	329.91	347.51	22.61			
		54786.39170	328.73	346.32	22.76	2008.8772	117.03	35.24
	2	55105.79028	VEGA			2009.7500	232.57	24.68
	3	55111.30572	321.05	30.97	23.42			
55111.35179		326.94	20.93	21.19				
55111.36393		274.44	136.19	9.62				
55111.42817		303.61	51.56	27.38	2009.7670	245.23	28.61	
	4	55115.27366	278.40	335.77	$\lesssim 5$			
55115.28937		320.12	31.97	25.14				
55115.32751		325.76	23.82	20.66				
55115.37560		311.93	63.05	29.19				
55115.42699		300.57	43.31	26.79				
55115.43530		250.00	119.11	18.47	2009.7780	246.85	29.20	
	5	55154.73407	VEGA			2009.8844	273.55	38.67
	6	55438.41255	305.46	82.90	29.03			
55438.42418		278.20	146.86	28.46				
55438.46260		275.30	137.64	30.17				
55438.46697		313.52	69.24	23.83				
55438.47285		328.00	197.39	$\lesssim 5$	2010.6626	290.61	33.43	
	7	55454.00139	VEGA			2010.7038	323.97	21.08
	8	55454.87917	VEGA			2010.7061	326.7	20.40
	9	55455.86944	VEGA			2010.7088	329.03	19.88
	10	55457.91458	VEGA			2010.7145	334.6	18.76

Table 1—Continued

System	Set	MJD	B(m)	$\vec{\theta}(\circ)$	$\vec{\rho}(\text{mas})$	<i>BY</i>	θ	$\rho(\text{mas})$
	11	55516.32097	257.29	302.44	30.37			
		55516.32602	301.64	229.43	24.33			
		55516.33092	329.67	0.80	$\lesssim 5$	2010.8758	92.36	34.30
	12	55775.47784	278.49	338.78	19.43			
		55775.48110	302.59	265.04	34.22			
		55775.48486	320.66	211.40	15.59			
		55775.51149	277.74	324.20	22.11			
		55775.51527	311.27	256.74	32.87			
		55775.51874	325.45	204.45	10.63	2011.5854	95.58	34.68
	13	55781.49346	154.89	244.53	30.45			
		55782.46689	278.48	330.58	22.70			
		55782.47149	305.21	263.10	35.57			
		55782.47329	322.23	209.56	10.47	2011.6038	100.54	36.77
	14	55796.47406	276.15	319.35	31.81			
		55796.47892	313.38	251.43	27.16			
		55796.51211	270.17	311.09	33.49			
		55796.52028	310.61	240.55	23.13			
		55796.52417	329.21	10.04	6.65	2011.6429	110.97	35.79
	15	55800.97014	VEGA			2011.6535	114.5	34.2
	16	55804.96875	VEGA			2011.6647	118.6	35.4
	17	55805.88541	VEGA			2011.6672	118.9	33.1
	18	55808.46680	272.65	313.75	31.24			
		55808.47141	312.76	245.12	17.29			
		55808.50026	264.68	306.72	30.95			
		55808.50324	307.61	236.24	13.31			

Table 1—Continued

System	Set	MJD	B(m)	$\vec{\theta}(^{\circ})$	$\vec{\rho}(\text{mas})$	BY	θ	$\rho(\text{mas})$
		55808.50705	329.49	6.49	13.86	2011.6757	121.93	31.60
19		55829.47895	250.59	299.36	22.27			
		55829.50961	233.92	293.38	18.36			
		55829.51409	287.85	35.10	6.51			
		55829.51668	329.25	350.38	21.15			
		55829.52144	226.52	291.16	20.43			
		55829.52630	283.85	30.66	10.55			
		55829.53052	328.91	347.48	22.42	2011.7333	144.56	23.69
20		55843.49748	216.41	288.40	$\lesssim 5$			
		55843.50346	279.11	24.35	19.48			
		55843.50806	328.28	343.87	19.45			
		55843.51536	276.47	20.22	17.64			
		55843.52185	327.40	340.47	19.57	2011.7716	191.92	20.37
21		55867.29442	313.52	69.06	22.35			
		55867.30024	245.53	311.21	$\lesssim 5$			
		55867.30339	300.65	19.59	21.09	2011.8367	222.95	23.90
22		56116.44410	246.26	357.45	16.04			
		56116.45118	256.82	53.23	20.39			
		56116.47894	246.99	347.41	17.32			
		56116.48838	274.66	46.99	20.55	2012.5189	210.97	21.51
23		56131.45171	273.39	99.73	20.98			
		56131.45494	305.70	41.85	24.49			
		56131.49109	296.31	88.93	26.17			
		56131.49745	318.16	33.86	25.23			
		56132.45407	276.90	98.03	23.39			

Table 1—Continued

System	Set	MJD	B(m)	$\vec{\theta}(^{\circ})$	$\vec{\rho}(\text{mas})$	BY	θ	$\rho(\text{mas})$
		56132.45923	308.15	40.61	24.86			
		56132.50179	278.50	152.50	$\lesssim 5$			
		56132.50395	302.85	84.85	25.19			
		56132.50918	321.02	31.00	24.37	2012.5615	242.73	27.70
	24	56141.49189	249.38	144.81	15.34			
		56141.49717	246.79	85.11	34.11			
		56141.50164	242.69	23.27	19.20			
		56141.52016	250.27	79.45	31.13			
		56141.52248	244.42	18.37	17.65	2012.5875	259.14	33.47
	25	56148.43688	278.27	157.68	10.26			
		56148.44204	294.83	89.75	34.02			
		56148.44580	316.78	35.03	24.53			
		56148.47143	306.04	82.42	35.55			
		56148.47361	322.59	29.09	23.85	2012.6065	261.45	35.76
	26	56186.39405	277.28	142.40	28.84			
		56186.39996	312.62	74.18	35.44			
		56186.40423	312.90	73.41	34.07			
		56186.40659	326.81	21.28	11.10			
		56186.43604	272.06	133.06	28.83			
		56186.44046	312.36	64.02	32.18			
		56186.44287	328.82	13.18	8.42	2012.7104	274.51	38.01
	27	56195.21723	227.81	131.78	36.77			
		56195.22068	275.90	51.78	21.07			
		56195.28974	277.82	163.08	20.49			
		56195.29970	287.67	93.39	35.59			

Table 1—Continued

System	Set	MJD	B(m)	$\vec{\theta}(\circ)$	$\vec{\rho}(\text{mas})$	<i>BY</i>	θ	$\rho(\text{mas})$
		56195.30585	313.91	37.18	13.40	2012.7347	288.68	37.08
	28	56244.28144	328.68	194.00	13.40			
		56244.38883	223.77	110.39	$\lesssim 5$			
		56244.39403	282.43	208.79	13.02			
		56244.39830	328.77	166.56	12.29	2012.8691	18.54	13.64
	29	56258.20213	312.46	254.56	21.69			
		56258.20854	276.38	139.89	$\lesssim 5$			
		56258.21204	326.93	200.95	13.11			
		56258.22187	313.53	249.55	20.71			
		56258.22972	328.07	197.05	16.21	2012.9070	55.74	20.42
HD 178911	1	54254.47802	176.18	329.48	67.38			
		54255.47226	106.82	269.34	49.17	2007.4219	315.85	71.1
	2	54287.38767	247.62	6.94	36.30			
		54287.39665	247.54	4.92	37.76			
		54287.40027	247.52	4.11	37.40			
		54287.45357	247.67	352.06	49.17			
		54287.46043	247.75	350.54	50.61			
		54287.46836	247.84	348.79	51.32			
		54287.47382	247.92	347.60	50.03			
		54287.48275	248.00	345.67	55.63			
		54289.27782	246.83	28.29	16.02			
		54289.28499	247.23	27.00	15.72			
		54289.35189	247.97	13.61	27.00			
		54289.36386	247.83	11.01	31.55	2007.5123	309.36	66.7
	3	54392.09675	276.09	311.99	29.46			

Table 1—Continued

System	Set	MJD	B(m)	$\vec{\theta}(\text{°})$	$\vec{\rho}(\text{mas})$	BY	θ	$\rho(\text{mas})$
		54393.16536	253.17	300.86	33.25			
		54393.19627	234.44	296.94	35.04	2007.7994	269.81	41.8
	4	54605.41302	273.83	153.45	21.50			
		54605.44835	277.38	144.95	29.15	2008.3809	84.42	62.4
	5	54692.26049	329.96	15.39	46.61			
		54692.30746	328.76	4.52	35.94			
		54692.31519	266.47	125.32	37.51			
		54692.37147	329.33	349.38	18.42	2008.6186	65.69	73.7
	6	55115.12027	306.25	62.87	65.49			
		55115.17057	261.94	203.52	33.96	2009.7759	13.82	100.2
	7	55346.42248	330.60	25.43	71.25			
		55346.49629	302.75	60.40	28.54			
		55347.50372	398.76	57.86	31.77			
		55348.33696	320.94	39.30	57.82	2010.4113	349.10	88.5
	8	55439.16025	310.57	258.16	22.89			
		55439.16753	330.58	25.70	48.07			
		55440.13761	274.90	331.13	84.67			
		55440.14199	306.16	261.22	28.09			
		55440.14627	329.91	29.27	45.60	2010.6648	336.50	83.4
	9	55683.42156	269.16	344.42	12.75			
		55683.42480	278.59	91.21	34.96			
		55683.43068	323.54	37.65	16.14			
		55683.46464	274.02	153.04	19.76			
		55683.46827	303.69	82.51	37.97			
		55683.47289	329.42	30.61	18.74	2011.3334	272.75	39.0

Table 1—Continued

System	Set	MJD	B(m)	$\vec{\theta}(\circ)$	$\vec{\rho}(\text{mas})$	BY	θ	$\rho(\text{mas})$
	10	55750.31281	277.25	145.35	$\lesssim 5$			
		55750.31537	312.00	256.64	20.51			
		55750.31904	330.62	204.94	27.56	2011.5164	223.15	26.7
	11	55775.23804	276.69	146.90	23.91			
		55775.24174	310.84	257.91	$\lesssim 5$			
		55775.24487	330.52	206.16	21.37	2011.5847	168.89	26.2
	12	55781.16531	176.82	172.22	32.23			
		55781.16903	145.91	258.19	$\lesssim 5$			
		55781.17239	245.07	211.91	16.83			
		55781.29349	176.45	150.41	23.91			
		55781.30175	247.59	186.23	26.18	2011.6010	167.22	27.8
	13	55872.30055	274.54	130.32	21.41			
		55872.30607	301.97	239.88	$\lesssim 5$			
		55872.30953	329.91	187.74	25.97	2011.6040	163.22	26.9
	14	55796.13238	271.32	158.97	25.93			
		55796.13608	291.49	87.30	15.98			
		55796.13942	326.65	34.91	11.75			
		55796.17761	276.43	147.55	27.34			
		55796.18115	310.21	78.47	11.61			
		55796.18441	330.44	26.81	15.77	2011.6420	146.60	28.6
	15	55829.21391	262.59	123.76	38.91			
		55829.21798	283.22	48.92	18.39			
		55829.22325	328.64	178.01	19.64	2011.7324	114.23	40.8
	16	55843.12053	276.64	132.75	40.74			
		55843.12472	306.93	63.39	29.01			

Table 1—Continued

System	Set	MJD	B(m)	$\tilde{\theta}(^{\circ})$	$\tilde{\rho}(\text{mas})$	BY	θ	$\rho(\text{mas})$
		55843.21415	243.02	118.53	39.39			
		55843.21797	262.56	36.32	12.03			
		55843.22321	329.37	169.02	22.97	2011.7707	110.72	42.2
	17	56053.43557	148.95	76.07	78.33			
		56053.43978	176.95	352.70	42.81			
		56053.46060	247.45	26.14	73.31			
		56053.46509	154.22	70.67	80.67			
		56053.46718	177.24	346.38	34.27	2012.3460	54.23	82.81
ξ Cep	1	53543.46805	264.15	145.30	43.01			
		53543.47206	263.59	144.16	46.18			
		53543.47332	263.41	143.81	50.25			
		53545.47370	307.21	81.13	28.31			
		53545.48238	308.57	78.34	27.74			
		53545.49434	310.16	74.51	24.02	2005.4770	134.74	47.05
	2	53605.26045	296.20	97.24	18.78			
		53605.26625	297.77	95.32	20.41			
		53605.27839	300.82	91.32	15.62			
		53605.28436	302.20	89.38	17.07			
		53605.29017	203.47	87.49	15.65			
		53606.26080	297.04	96.22	20.02			
		53606.27070	299.61	92.96	19.47			
		53606.28720	303.42	87.57	16.13			
		53606.29554	305.12	84.87	15.55			
		53606.30309	306.51	82.44	15.38			
		53607.21439	283.67	111.12	26.94			

Table 1—Continued

System	Set	MJD	B(m)	$\vec{\theta}(\text{°})$	$\vec{\rho}(\text{mas})$	BY	θ	$\rho(\text{mas})$
		53607.22045	285.68	109.00	24.27			
		53607.26000	297.56	95.58	18.34			
		53607.26623	299.17	93.52	18.24			
		53607.27263	300.75	91.42	16.33	2005.6462	149.64	32.98
	3	54956.46830	237.76	65.66	48.00			
		54956.47822	268.73	126.87	46.15			
		54956.48590	271.36	177.59	$\lesssim 5$	2009.3430	90.76	54.77
	4	55054.33274	215.59	26.97	17.70			
		55054.34009	216.80	24.89	16.13			
		55054.40038	222.38	189.93	$\lesssim 5$			
		55055.28509	207.29	37.79	26.73			
		55055.28923	208.12	36.98	20.92			
		55055.29340	209.01	35.97	22.73			
		55055.37557	220.88	15.56	$\lesssim 5$			
		55055.37994	221.23	14.46	$\lesssim 5$	2009.6126	101.87	57.39
	5	55111.34328	301.45	169.10	37.03			
		55111.38765	308.39	194.63	12.62			
		55111.42014	307.59	182.87	23.81			
		55115.25704	243.85	119.36	58.03			
		55115.28199	302.85	182.07	26.14			
		55115.36752	308.77	197.85	9.83	2009.7725	117.67	58.40
	6	55438.36362	246.65	301.95	17.27			
		55438.36833	313.51	236.62	53.89			
		55438.37562	302.17	187.78	36.17			
		55438.43415	220.71	281.79	32.75			

Table 1—Continued

System	Set	MJD	B(m)	$\vec{\theta}(^{\circ})$	$\vec{\rho}(\text{mas})$	BY	θ	$\rho(\text{mas})$
		55438.43678	311.23	213.59	49.53	2010.6624	231.84	52.25
	7	55445.15468	159.94	189.88	33.80			
		55445.15817	190.54	232.51	50.10			
		55445.16096	133.46	287.40	27.15			
		55445.21604	206.99	218.23	49.73	2010.6810	232.73	49.38
	8	55808.43387	216.69	97.81	64.91			
		55808.43643	310.52	29.34	25.49			
		55808.44095	301.06	167.75	20.26	2011.6756	96.07	64.85
	9	55829.35906	222.01	102.67	66.09			
		55829.36364	248.44	38.73	30.14			
		55829.36755	245.04	164.84	26.88			
		55829.39391	205.69	92.04	64.86			
		55829.39839	246.21	26.67	17.60			
		55829.40049	240.86	156.47	36.77	2011.7329	100.50	65.30
	10	55843.33283	217.05	99.36	64.08			
		55843.33683	247.73	34.96	24.74			
		55843.34008	243.83	161.97	32.45	2011.7711	102.31	64.18
	11	55892.08110	256.78	133.23	58.82			
		55892.08577	311.75	69.51	51.06			
		55892.08983	298.41	18.97	$\lesssim 5$	2011.9046	108.18	65.13
	12	56082.47286	268.72	157.91	36.61			
		56082.47817	239.11	102.02	18.91			
		56082.48203	234.60	211.85	22.50			
		56082.48501	267.71	154.38	34.86			
		56082.48968	241.40	98.10	18.01			

Table 1—Continued

System	Set	MJD	B(m)	$\vec{\theta}(\circ)$	$\vec{\rho}(\text{mas})$	BY	θ	$\rho(\text{mas})$
		56082.49370	236.95	209.07	25.80	2012.4259	160.69	36.52
	13	56195.17156	268.15	155.83	21.53			
		56195.17708	297.96	275.08	22.59			
		56195.18340	282.85	218.48	42.76			
		56195.26650	253.28	128.91	$\lesssim 5$			
		56195.27046	312.76	244.77	38.53			
		56195.27504	300.08	195.12	38.15	2012.7345	217.45	42.63
	14	56245.21508	224.56	284.41	30.82			
		56245.22044	311.68	216.35	48.13			
		56245.22627	302.20	172.42	24.72	2012.8714	232.62	50.00

Note. — Observation log for ω Andromeda, HD 178911, and ξ Cephei on the CHARA Array from 2005 to 2012. Each set of vector observations (along with the projected baseline length and epoch of observation) in columns 3 – 6 were combined to create the true location of the secondary and average time of all the data points defined in the last three columns. Errors for all measurements in the final column are ≈ 1 mas.

Table 2. ω Andromeda Orbital Elements and Calculated Values.

Elements	This Paper
P (days)	254.9003 ± 0.1960
(yr)	0.69789 ± 0.00054
T ₀ (MJD)	54214.835 ± 3.187
(BY)	2007.3110 ± 0.0087
a (")	0.038 ± 0.001
e	0.142 ± 0.012
i (°)	62.49 ± 2.10
ω (°)	278.87 ± 2.01
Ω (°)	115.94 ± 4.38
K ₁ (km/s)	17.54 ± 0.30
K ₂ (km/s)	19.62 ± 0.30
γ_0 (km/s)	14.83 ± 0.17
$\chi^2_{\nu}(\text{RV})$	106.53
$\chi^2_{\nu}(\text{VIS})$	15.59
$\chi^2_{\nu}(\text{Combined})$	84.29
$M_{\text{P}} (M_{\odot})$	0.993 ± 0.056
$M_{\text{S}} (M_{\odot})$	0.888 ± 0.058
π_{orb} (")	0.03912 ± 0.00197
π_{Hip} (")	0.03494 ± 0.0031

Table 3. HD 178911 Orbital Elements and Calculated Values.

Elements	Tokovinin (2000)	This Paper
P (days)	1296.3 ± 1.1	1296.984 ± 0.355
(yr)	3.55 ± 0.003	3.55102 ± 0.00097
T ₀ (MJD)	50572.2 ± 1.5	50574.953 ± 1.302
(BY)	1997.337 ± 0.00411	1997.34538 ± 0.00356
a(")	0.0735 ± 0.0026	0.074 ± 0.002
e	0.589 ± 0.004	0.597 ± 0.003
i (°)	150.1 ± 3.7	147.29 ± 0.99
ω (°)	262.5 ± 0.8	83.88 ± 0.87
Ω (°)	276.7 ± 1.5	276.91 ± 1.45
K ₁ (km/s)	6.57 ± 0.04	6.47 ± 0.09
K ₂ (km/s)	8.53 ± 0.17	8.33 ± 0.18
γ_0 (km/s)	-41.01 ± 0.03	-41.04 ± 0.06
χ^2_{ν} (RV)		0.685
χ^2_{ν} (VIS)		2.187
χ^2_{ν} (Combined)		0.997
M_P (M_{\odot})	1.07 ± 0.37	0.802 ± 0.055
M_S (M_{\odot})	0.84 ± 0.29	0.622 ± 0.053
π_{orb} (")	0.025 ± 0.008	0.02826 ± 0.00170

Table 4. ξ Cephei Orbital Elements and Calculated Values

Elements	Pourbaix (2000)	This Paper
P (days)	818.51 ± 0.98	819.9402 ± 0.6082
(yr)	2.241 ± 0.0027	2.24492 ± 0.00167
T ₀ (MJD)	40949.584 ± 3.36	40949.144 ± 3.973
(BY)	1970.992 ± 0.0092	1970.9908 ± 0.0105
a(")	0.072 ± 0.0017	0.074 ± 0.004
e	0.50 ± 0.021	0.481 ± 0.024
i (°)	68 ± 1.4	70.96 ± 1.72
ω (°)	273 ± 1.1	272.98 ± 1.95
Ω (°)	85 ± 1.9	89.64 ± 3.51
K ₁ (km/s)	7.16 ± 0.56	7.81 ± 0.50
K ₂ (km/s)	19.82 ± 0.55	19.98 ± 0.83
γ_0 (km/s)	-10.74 ± 0.34	-10.59 ± 0.33
χ^2_{ν} (RV)		204.65
χ^2_{ν} (VIS)		45.01
χ^2_{ν} (Combined)		150.55
M_P (M_{\odot})	1.00 ± 0.13	1.045 ± 0.032
M_S (M_{\odot})	0.36 ± 0.05	0.409 ± 0.066
π_{orb} (")	0.038 ± 0.0021	0.03811 ± 0.00282

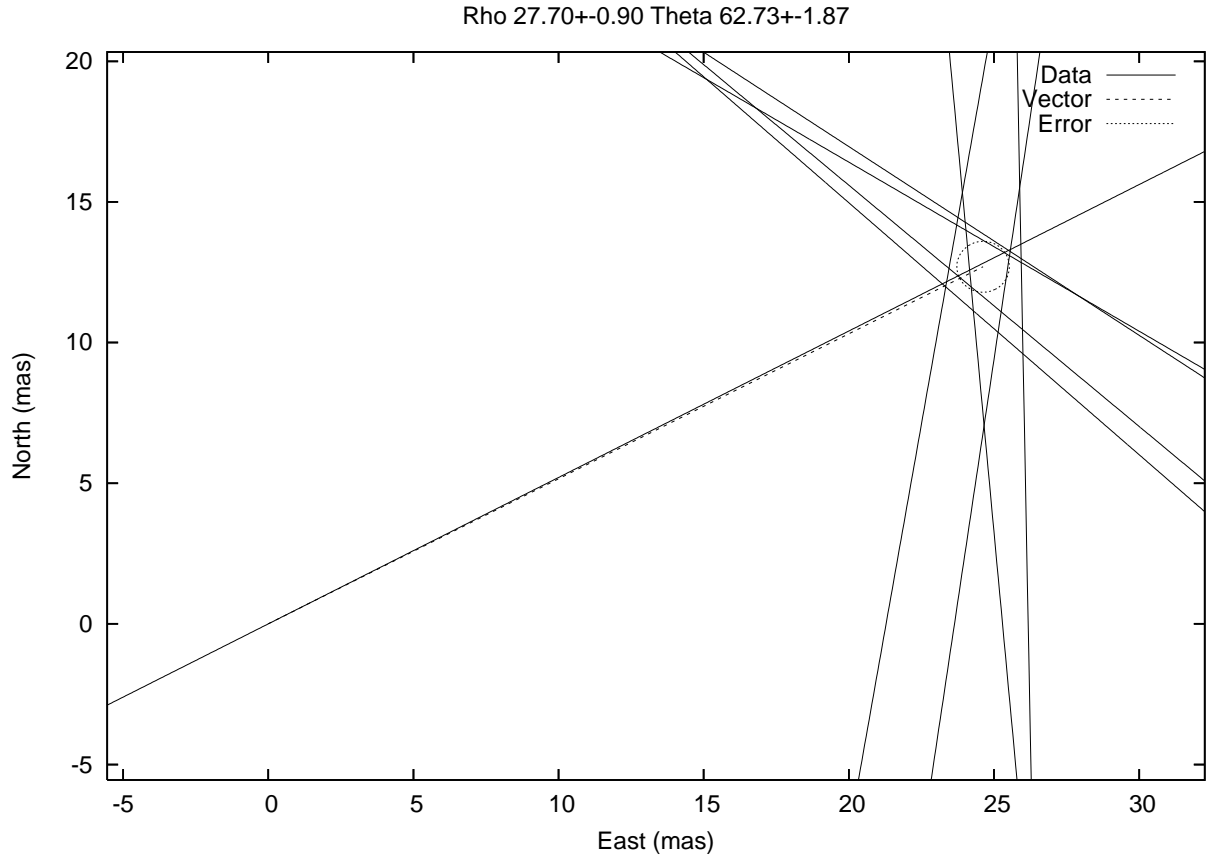


Fig. 1.— Example Vector Separation Plot for ω Andromeda, 2012.5615. An example output from the SFPAstrom program that solves for the location of the companion from multiple 1-D vector measurements. The dashed line is the vector from the origin to the estimated location of the companion. Each solid line is one 1-D vector measurement, and the dashed circle is the error ellipse for the best estimate for the position of the secondary and the size of the ellipse represents the error of the secondary position.

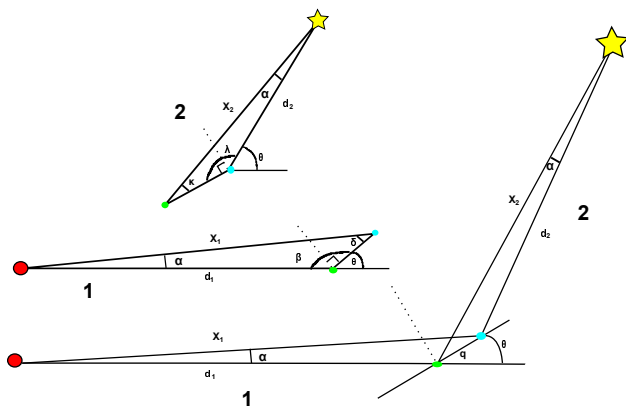


Fig. 2.— Simple diagram of the components comprising beam path from the beam combiner to the observed system. The distances χ_1 and χ_2 are the misaligned paths when d_1 and d_2 are the optical axis when the alignment is done correctly, α is the angle subtended by the path difference between the beam combiner and the telescope, and θ is the angle of the telescope with 0 at zenith and 90 at the horizon. The difference between the χ and d paths is calculated in terms of α and θ .

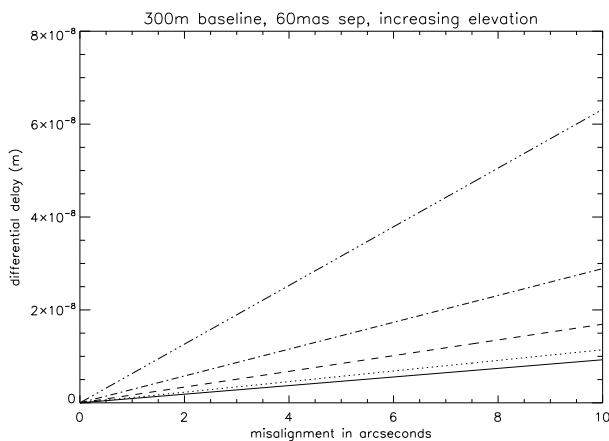


Fig. 3.— Calculated differential delay based on telescope angle and realistic beam misalignment. The lines correspond to angles from near the horizon to near zenith (solid line near zenith, each line after decreases the zenith angle by 15 degrees, ending at 30 degrees above the horizon) and represent the difference between the single and double star cases described in Equation 8 compared to the ideal path case of approximately $1\mu\text{m}$.

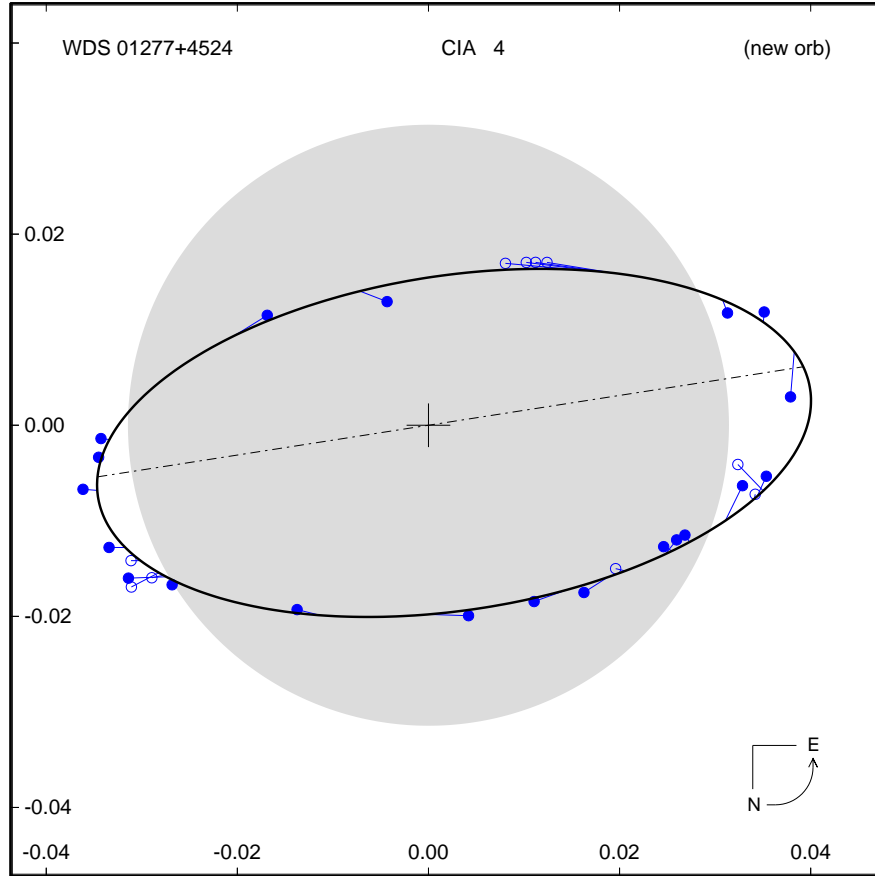


Fig. 4.— Orbit Plot for ω Andromeda. Combined visual-spectroscopic solution from this paper (solid line) using all available data which is all from the CHARA Array SFP Program. The shaded circle represents the resolution limit of a speckle interferometry camera on a 4-m telescope and is shown to aid in scaling. The dot-dash line indicates the line of nodes. The VEGA beam combiner measures are shown as open circles. The CHARA Array SFP measures are indicated with filled circles. All measurements are connected to their predicted positions on the orbit by “O–C” lines. The direction of motion is indicated on the north-east orientation in the lower right of the plot. The scales at left and bottom are in arcseconds.

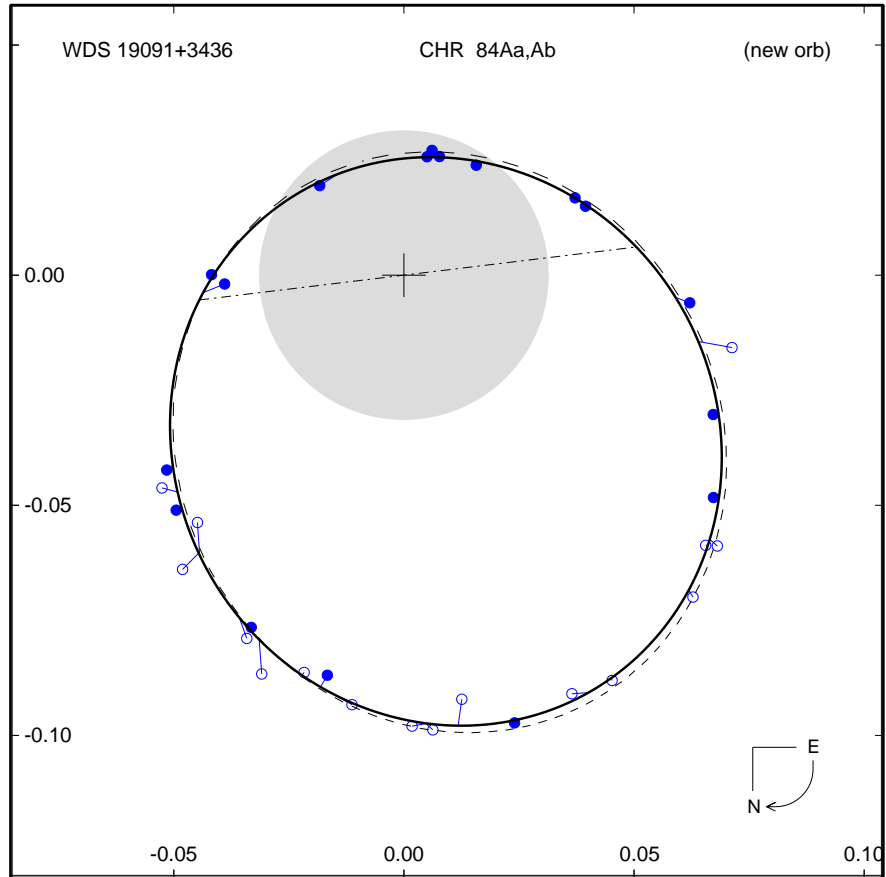


Fig. 5.— Orbit Plot for HD 178911. Combined visual-spectroscopic solution from this paper (solid line) using all available data which is consistent with the previous orbit of Tokovinin et al. (2000) (dashed line). The shaded circle represents the resolution limit of a speckle interferometry camera on a 4-m telescope. The CHARA Array SFP measures are indicated with filled circles. Speckle interferometry measurements are indicated as open circles. Other symbols as Figure 4.

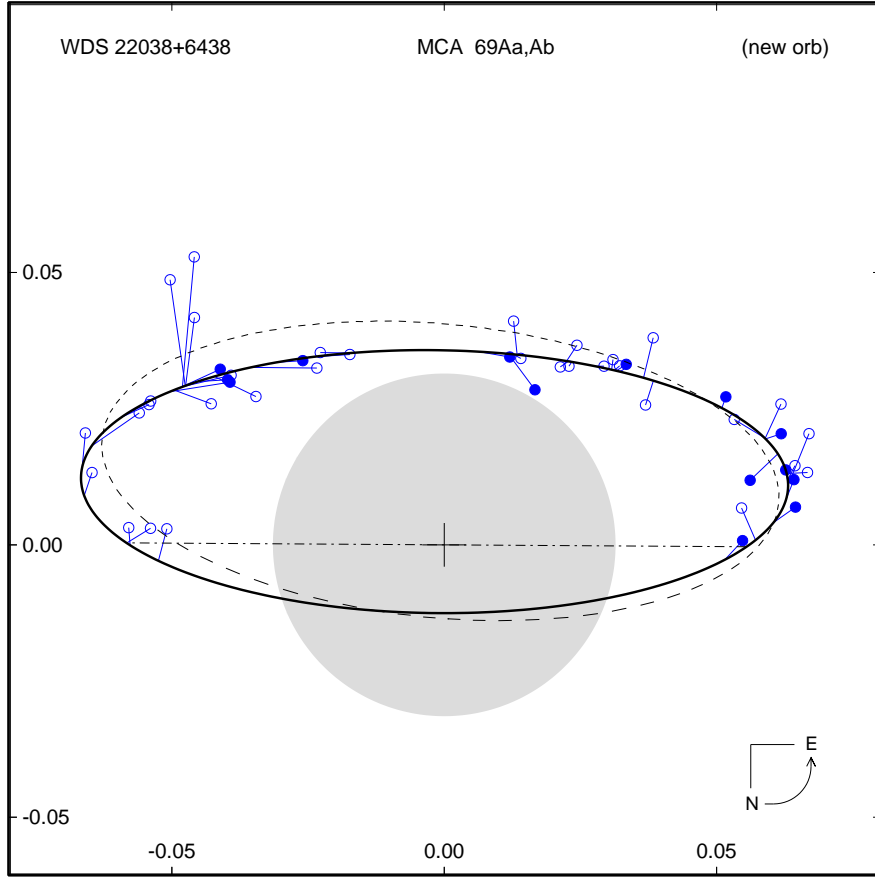


Fig. 6.— Orbit Plot for ξ Cephei. The figure shows the relative visual orbit of the system; the x and y scales are in arcseconds. The solid curve represents the orbit determined in this paper with the dashed curve denoting the orbit of Pourbaix (2000). Other symbols as Figure 5.